Concomitant Polymorphism of o-Aminobenzoic Acid in Antisolvent Crystallization

ARTICLE *in* CRYSTAL GROWTH & DESIGN · DECEMBER 2007

Impact Factor: 4.89 · DOI: 10.1021/cg070517n

3 AUTHORS, INCLUDING:

J.H. Ter Horst
University of Strathclyde
87 PUBLICATIONS **1,246** CITATIONS

SEE PROFILE

Part of the Special Issue: *Facets of Polymorphism in Crystals*

CRYSTAL GROWTH & DESIGN
2008
VOL. 8, NO. 1
37–43

Concomitant Polymorphism of *o*-Aminobenzoic Acid in Antisolvent Crystallization

Shanfeng Jiang,* Joop H. ter Horst, and Peter J. Jansens

Process & Energy Laboratory, Delft University of Technology, Leeghwaterstraat 44, 2628CA Delft, The Netherlands

Received June 7, 2007; Revised Manuscript Received September 7, 2007

ABSTRACT: Concomitant polymorphism is the result of an interplay between thermodynamics and kinetics. By understanding this interplay and the effect of operational factors on it, concomitant polymorphism can be avoided, and product quality can be improved. Antisolvent crystallization of *o*-aminobenzoic acid (*o*-ABA) was performed in batch experiments at 298 K by rapidly mixing an ethanol solution of *o*-ABA with water as antisolvent. At low initial supersaturations the stable form I crystallizes, while at high initial supersaturations the metastable form II crystallizes. At intermediate initial supersaturations, concomitant polymorphism occurs. It was observed that at higher supersaturations, form II has a higher growth rate than does form I, while the reverse occurs at lower supersaturations. At intermediate supersaturations, the growth rates of both forms are similar, and a nucleation assessment indicates that nucleation rates are similar as well. It was therefore concluded that not the solvent-mediated transformation but rather concomitant crystallization is responsible for the observed concomitant polymorphs. When all supersaturation toward form II is depleted, the solvent-mediated transformation starts. The solvent-mediated transformation of form II to form I is quite rapid, even at high water fraction. Pure form I is readily obtained by allowing sufficient time for the polymorph transformation to finish.

Introduction

Polymorphs differ in their physicochemical properties. To control the formation of polymorphs during production, for example, to avoid concomitant polymorphs,[1] is crucial in the chemical manufacture, especially in the pharmaceutical industry where consistency and reliability are of importance. Concomitant polymorphs can be responsible for the stability and bioavailability issues in pharmaceutical products. It is usually very difficult to achieve control, because polymorph crystallization is a delicate and complicated process essentially determined by thermodynamics, kinetics, and fluid dynamics. Therefore, to control polymorphic crystallization, it is necessary to understand, predict, and control the nucleation, crystal growth, and the effect of fluid dynamics.

In antisolvent crystallization, a model compound solution and an antisolvent that decreases the solubility are mixed. By varying both initial supersaturation ratio and antisolvent fraction not only the nucleation rate but also the growth rate will change. How the nucleation rate and growth rate of different polymorphs compete for the available supersaturation will determine the product quality, for example, the polymorphic fraction. In some cases, the polymorph transformation plays an important role in determination of the product quality as well.

The objective of this study is to understand the effect of supersaturation ratio and antisolvent fraction on the polymorphic crystallization behavior and the solvent-mediated transformation. The model compound is *o*-aminobenzoic acid (*o*-ABA), whose molecular structure is shown in Figure 1. It is typically used as an intermediate for production of dyes, pigments, and saccharin, and in preparing perfumes as well as pharmaceuticals.

* To whom correspondence should be addressed. E-mail: S.Jiang@tudelft.nl. Phone: +31 15 27 86 605. Fax +31 15 27 86 975.

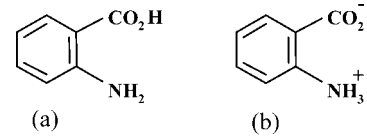

Figure 1. Molecular structure of *o*-aminobenzoic acid (*o*-ABA); nonzwitterions (a) and zwitterions (b).

o-ABA is known to crystallize in three forms.[2–4] Its polymorphic system exhibits enantiotropic behavior, with a transition temperature 354 K.[2] Form I is stable below 354 K and has two different molecules in the asymmetric unit cell: a nonzwitterionic molecule and a zwitterion shown in Figure 1, panels a and b, respectively. Above 354 K form II, which is only composed of nonzwitterionic molecules, is stable. Like form II, the form III structure only contains nonzwitterionic molecules. Form III could be obtained by condensation from the gas phase or by melt crystallization.[4]

Theory

Supersaturation for Antisolvent Crystallization. The driving force for crystallization is the supersaturation $\Delta\mu$ defined as $\Delta\mu = \mu_s - \mu_c$, where μ_s and μ_c are the chemical potentials in the solution and in the bulk of the crystal phase, respectively. When $\Delta\mu > 0$, the solution is supersaturated, and nucleation and crystal growth can occur. The supersaturation can be rewritten as $\Delta\mu = kT \ln S_a$, where k is the Boltzmann constant, and T is the absolute temperature. The supersaturation ratio is based on activity and defined as $S_a = a/a_e$ where a is the actual activity and a_e is the equilibrium activity. In antisolvent crystallization, the supersaturation is generated by the addition of an antisolvent which decreases the equilibrium activity of

10.1021/cg070517n CCC: $40.75
Published on Web 12/12/2007

solute in solution. Since the addition of the antisolvent also dilutes the solution, the decrease in equilibrium activity should largely exceed this dilution effect. Because the activity coefficients are not known and affected by speciation in the solution, for convenience the supersaturation ratio is simplified in terms of concentration:

$$S = \frac{c}{c^*} \tag{1}$$

with c the actual concentration and c^* the equilibrium concentration at a certain antisolvent fraction.

Nucleation. To estimate the homogeneous and heterogeneous nucleation rates the classical nucleation theory is used:[5]

$$J = A \exp\left[\frac{-W^*}{kT}\right] \tag{2}$$

where A is the pre-exponential kinetic parameter and W^* the nucleation work. For homogeneous nucleation (HON), the nucleation work, assuming spherical nuclei, is expressed as:

$$W^* = -\frac{16\pi\gamma^3 v^2}{3k^2T^2(\ln S)^2} \tag{3}$$

with v the molecular volume and γ the interfacial energy. The interfacial energy for HON is estimated by assuming a spherical nucleus from the bulk solubility c^* and molecular volume v according to the Mersmann equation[6] with the constant 0.514 from Kashchiev:[5]

$$\gamma = 0.514kT\frac{1}{v^{2/3}}\ln\frac{1}{vc^*} \tag{4}$$

For heterogeneous nucleation (HEN), the interfacial energy is replaced by an effective interfacial energy γ_{ef} defined as[5]

$$\gamma_{ef} = \psi\gamma \tag{5}$$

with the activity factor $0 < \psi < 1$. Since $\gamma_{ef} < \gamma$, the nucleation work for HEN is reduced considerably compared to that for HON, if active heterogeneous centers are presented in the system. The nucleation rate (eqs 2 and 3) indicates that for antisolvent crystallization of *o*-ABA, in which the temperature T is constant, two main variables govern the rate of nucleation: degree of supersaturation and (effective) interfacial energy.

Crystal Growth. The crystal growth is a two-step process involving the diffusion of the molecules from the bulk solution toward the crystal surface and surface integration of the molecule into the crystal lattice.[7] The general expression of growth rate is

$$R = k_G(\ln S)^n \tag{6}$$

where n is the growth order, which depends on the different growth mechanisms, and k_G is an overall growth constant coefficient. For surface integration k_G is a complex parameter, depending on the step free energies that can be related to the interfacial energy influenced by the antisolvent fraction. Therefore, like the nucleation rate, the growth rate of a crystal surface is also affected by supersaturation ratio and antisolvent fraction.

Induction Time. The induction time gives important information of nucleation and crystal growth rates. The induction time is the period of time between the achievement of supersaturation and the detection of crystals. Since a sufficient amount of crystals have to nucleate and grow up to a detectable size, it is a function of nucleation rate J and growth rate R.[5]

$$t_{ind} = \left(\frac{3\alpha}{\pi JR^3}\right)^{1/4} \tag{7}$$

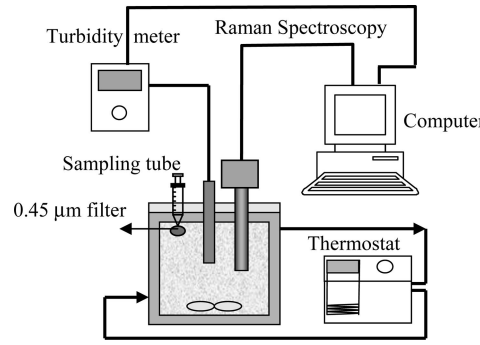

Figure 2. Experimental setup for antisolvent crystallization and inline measurements of transformation and solubility of form II.

Here α is the detectable volume (or mass) fraction of the new crystalline phase formed in the solution.

Experimental Section

Materials and Instrumentation. Purchased *o*-ABA (Fluka Chemie, chemical purity ≥99.5%) confirmed as form I by X-ray powder diffraction (XRPD), pure ethanol (chemical purity 100%), and ultra pure water were used in all experiments. As shown in Figure 2, the experiments of antisolvent crystallization, transformation, and solubility measurements of form II were preformed in a jacket glass crystallizer (200 mL), which was connected to a Haake thermostat to control the temperature at 298 K. A magnetic plate and stirrer were used for stirring the solution. A Hololab Series 5000 Raman spectroscopy (Kaiser Optical System, Inc.) was applied to record Raman spectra. A turbidity transmitter (InPro8200/S; Mettler Toledo) probe was inserted into the solution for measuring the induction time.

Solubility of Form I. The solubility of *o*-ABA form I in water/ethanol at 298 K was measured as a function of the water volume fraction in the range $x_{v,w} = 0$ to 1. Excess amounts of form I were dissolved in 20 mL mixed solvent of water/ethanol to saturate the solutions. After 4 days in a shaking bath (Julabo) at 298 K, the suspensions were filtered over a 0.22 μm filter. Samples of the saturated solutions were dried at 323 K until the solvent completely evaporated. The solubility was determined from the mass of the remaining crystalline material.

Antisolvent Crystallization of *o*-ABA Polymorphs. The formation of *o*-ABA polymorphs was investigated in the antisolvent crystallization with ethanol as solvent and water as antisolvent. The variation of supersaturation ratio and interfacial energy was achieved by changing both the initial concentration of *o*-ABA in ethanol ($c_{o\text{-ABA}} = 0.73$–1.2 mol/L-solution) and water volume fraction ($x_{v,w} = 0.4$–0.8). The total volume of antisolvent and solvent for each experiment was 100 mL. *o*-ABA solution was prepared by dissolving the corresponding amount of *o*-ABA in ethanol and stirring for 1 h. Into the setup shown in Figure 2, the *o*-ABA solution and the corresponding amount of water were synchronously added under a constant stirring speed (500 rpm). In situ Raman spectra were recorded every minute to identify the obtained polymorph. The induction times were measured by recording the turbidity every second. A microscope was further used to identify the two polymorphs due to their distinct morphology.

Solubility of Form II and Inline Transformation Measurement. The solubility measurement procedures of form I cannot be applied to form II because of a relative fast solvent-mediated transformation from form II into I. For the solvent-mediated transformation, the general features of the supersaturation−time profiles are described as three steps.[8] First, a decrease of concentration from the initial value occurs because of the nucleation and growth of stable form I. Second, there is a concentration plateau during which the growth and dissolution processes are balanced. Finally, a further reduction of concentration takes place when the form II has completely dissolved, and form I finishes its growth.

Raman spectroscopy was applied to observe the transformation process. The solubility of form II and the transformation rate were studied at $x_{v,w} = 0.6$, 0.7, and 0.8. The concentration of *o*-ABA solution was 1.16 mol/L-solution, and the total volume of solvent and antisolvent

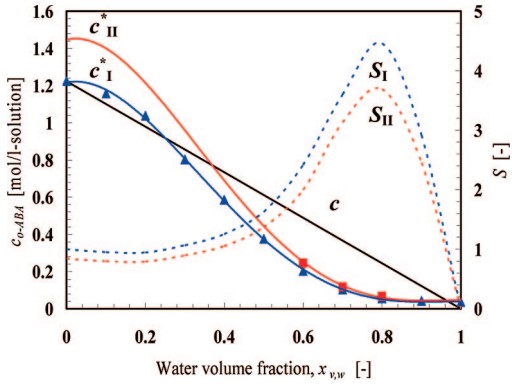

Figure 3. Solubility curves of *o*-ABA as a function of water volume fraction at 298 K. (▲) form I; (■) form II. Solid Lines (c^*_I and c^*_{II}) are trendlines of both forms. The trendline of c^*_{II} was estimated with the value of $c^*_{II}/c^*_I = 1.20$ at $x_{v,w} = 0.6$–0.8. Solid-straight line (c) shows the working line as a function of water volume fraction. Dashed lines are supersaturations S_I and S_{II} determined by the ratio between the working line and the solubility curves of both forms under the assumption of perfect mixing.

was 100 mL for $x_{v,w} = 0.6$, 0.7, and 135 mL for $x_{v,w} = 0.8$. The crystal suspensions of form II were obtained by mixing the *o*-ABA solution and corresponding amount of water into the setup shown in Figure 2 using the same procedure described in antisolvent crystallization. The theoretic yield of form II was estimated around 3 g. Raman spectra were recorded every minute. During an experiment a 5 mL sample of the clear solution was taken using a pipet connected with a 0.45 μm filter, as soon as a decrease of Raman intensity of form II (shown in Figure 8) was observed, indicating that the concentration plateau was established. By making the just assumption that the dissolution of form II is much faster than the growth of form I the concentration plateau is equal to the solubility of form II. This clear solution was dried in an oven at 323 K until the solvent was completely evaporated. The solubility of form II was determined from the mass of the remaining crystalline material.

Growth Rate Measurement. An *o*-ABA solution in ethanol with the concentration of 1.2 mol/L-solution was mixed with water at volume fraction of 0.5 in a jacket glass crystallizer kept at 298 K. To observe the entire crystallization process under the microscope, the mixing time must be shorter than the induction time but should be long enough to make sure the reactants mix completely. After the solution was mixed approximately 30 s, a droplet of this well-mixed and clear solution was immediately moved into a glass stage positioned under the microscope. Microscopic images were taken every 10 s using the software of Image-Pro Plus (Media Cybernetics). In this way, the sequence of microscopic images recorded the entire crystallization process, including the appearance, growth, and transformation of crystals.

Experimental Results

Solubility of Forms I and II. The solubility data of form I at $x_{v,w} = 0$ – 1 and of form II at $x_{v,w} = 0.6$–0.8 are presented in Figure 3. A higher solubility of form II can be observed, which confirms form II is the metastable form. The stable form I was very soluble in pure ethanol, $c^*_I = 1.22$ mol/L-solution at $x_{v,w} = 0$. Its solubility decreased with increasing water volume fraction. In pure water, it was only slightly soluble, $c^*_I = 0.04$ mol/L-solution. The average value of c^*_{II}/c^*_I at $x_{v,w} = 0.6$–0.8 was approximated to 1.20.

The chemical potential of the stable form is lower than that of the metastable form. For the solid phases of forms I and II in contact with their equilibrium solution, $\mu_0 + RT \ln a_I < \mu_0 + RT \ln a_{II}$, where μ_0 is the standard chemical potential and a is the solution activity. Therefore, $a_I < a_{II}$, and since activity a is related to concentration c^* and activity coefficient γ_a, $c^*_I \gamma_{aI} < c^*_{II} \gamma_{aII}$. By assuming $\gamma_{aI}/\gamma_{aII} = 1$ at any mixed-composition

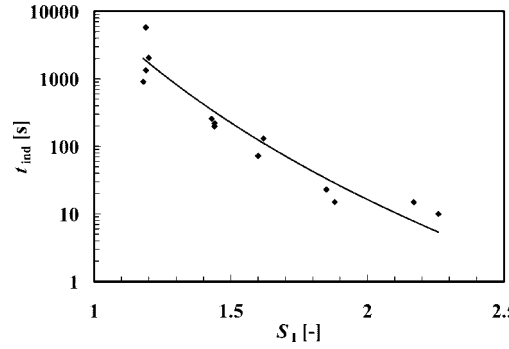

Figure 4. Induction time t_{ind} as a function of initial supersaturation ratio S_I.

of water/ethanol system, the solubility ratio c^*_I/c^*_{II} should be a constant at any given water/ethanol fraction.

With the value for c^*_{II}/c^*_I at $x_{v,w} = 0.6$ – 0.8, the overall solubility curve of form II was estimated and shown in Figure 3. The solubility ratio c^*_{II}/c^*_I of *o*-ABA was larger than that of L-histidine, $c^*_B/c^*_A = 1.08$.[9] This larger solubility difference could result in a faster transformation process of *o*-ABA.

In Figure 3, a typical working line, c, is presented together with the solubility curves. The corresponding concentration-based supersaturation ratios (eq 1) for both forms under the assumption of perfect mixing are shown as well. Because of the lower solubility of form I, an overall higher supersaturation ratio can be achieved. The created supersaturation is a trade off between a decrease in concentration due to dilution and a decrease in solubility due to the antisolvent fraction. Both S_I and S_{II} are increasing with an increase of water volume fraction up to approximately $x_{v,w} = 0.8$. For further increase of the water volume fraction, the supersaturation ratios eventually decrease again until for $x_{v,w} = 1$, S_I and $S_{II} = 0$.

Induction Time versus Mixing Time. The induction time versus the initial supersaturation ratio S_I is presented in Figure 4. A decreasing trend of induction time with the supersaturation ratio can be seen, although it should be noted that the antisolvent fraction was also varied. It varies from 95 min at $S_I = 1.2$ to approximately 10 s at $S_I = 2.3$. Care was taken that solution and antisolvent were mixed rapidly, $t_m < 1$ s. The shortest induction time was longer than the mixing time in the batch experiment. It therefore can be assumed that the crystallization occurs in a homogeneously mixed solution, that is, the nucleation and crystal growth started at a uniform supersaturation in the crystallizer.

Raman Spectra. Raman spectra of pure form I and II were respectively recorded using the purchased material (form I) and using dry samples from experiments of antisolvent crystallization. The Raman spectrum of form III is also presented in Figure 5 and its preparation from solution will be reported in a forthcoming paper. These three polymorphs were all confirmed as pure forms I, II, or III by XRPD. As shown in Figure 5a, compared to forms II and III, the Raman spectrum of form I is quite different. For instance, form I has unique peaks in the ranges of 900–1000 cm^{-1} and 1350–1420 cm^{-1}, and the two peaks of form I in the range of 735–814 cm^{-1} are also apparently different from the other two forms. Forms II and III have very similar spectra, and a number of small differences are indicated by arrows in Figure 5a. The reason for these spectra differences is that form I has both zwitterions and nonzwitterions, while forms II and III are only composed of nonzwitte-

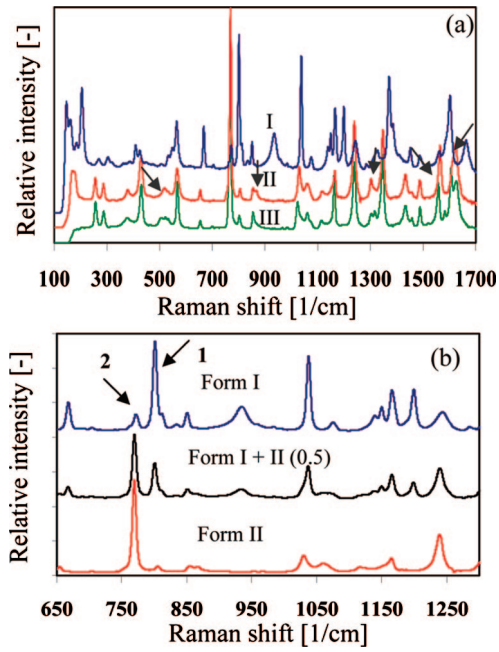

Figure 5. (a) Raman spectra of pure forms I, II, and III. Arrows indicate differences between forms II and III. (b) Raman spectra between 650 and 1250 cm^{-1} shift of pure forms I and II and of a mixture of both polymorphs with 0.5 weight fraction. Peaks 1 and 2 are used to determine the polymorphs for forms I and II.

rions. Raman spectra of crystal samples from the experiments described in this paper never showed indication of the presence of form III.

Figure 5b shows spectra differences between forms I and II in the range of 650–1250 cm^{-1}. Peak 1 in the range of 793–814 cm^{-1} and peak 2 in the range of 735–790 cm^{-1} are characteristic for respectively forms I and II. The intensity of peak 1 is quite low for form II, but increases with increasing the fraction of form I. The intensity of peak 2 is high for form II, but decreases with an increase of the fraction of form I. The middle spectrum was recorded using a dry mixture of the two forms with a weight fraction of 0.5. It illustrates how these two peaks change with the polymorphic fraction. Using Raman spectra, the polymorphic fraction can be determined both inline and offline.

Formation of Polymorphs from Antisolvent Crystallization. According to eq 1 the supersaturation ratio is increased either by increasing the initial concentration of *o*-ABA in ethanol solution or by decreasing the solubility through increasing the water volume fraction. On the basis of eq 4 the interfacial energy increases with the water volume fraction. In turn, both the supersaturation and interfacial energy affect nucleation and growth of the polymorphs. In this study the initial supersaturation ratio S_I was varied from 1.2 to 4.5 and the water volume fraction was varied from 0.38 to 0.8, which related to interfacial energy $\gamma = 20.0-37.8$ mJ/m^2.

Forms I and II were readily obtained in the antisolvent crystallizations, while form III was never observed. In Figure 6, the polymorph that was identified just after the induction time at different initial supersaturation ratios S_I (1.0−2.5) and water volume fractions $x_{v,w}$ (0.35−0.65) is shown.

When $S_I = 1.2$, only form I was obtained at all used water volume fractions. The induction time was rather scattered: from 15 to 95 min as shown in Figure 4.

Concomitant polymorphism was observed at $S_I = 1.4$ and 1.6 right after the induction time. Induction times from 70 to

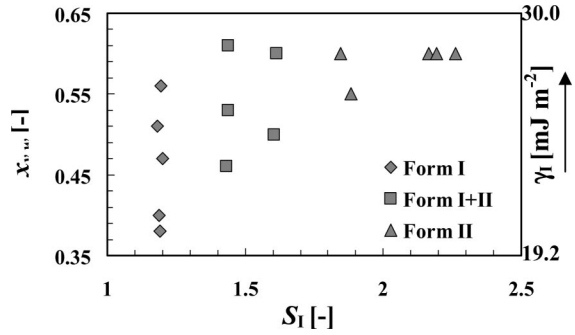

Figure 6. Polymorphs identified just after the first observation of crystals using microscopy as a function of the initial supersaturation ratio S_I and water volume fraction $x_{v,w}$. Interfacial energy γ increases with $x_{v,w}$ from 19.2 to 30.0 mJ/m^2.

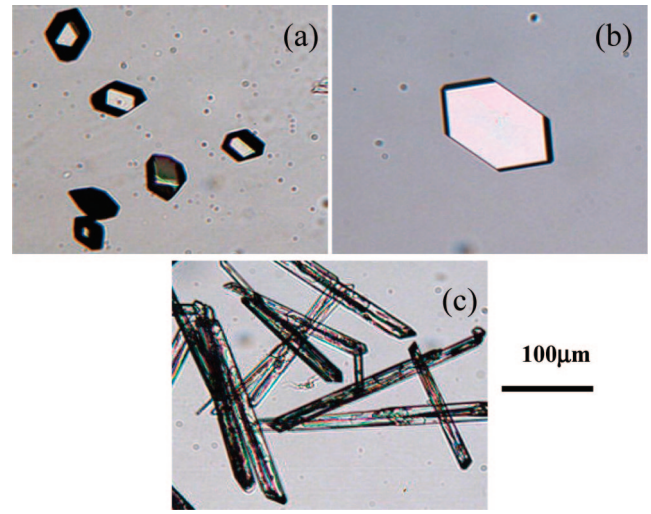

Figure 7. Crystals of form I (a), form II with plate shape (b) and with needle shape (c).

260 s were reported. The mixture contained small fractions of form II with a platelike shape.

As S_I was further increased to 1.9−2.3, the induction time was around 10−20 s, and the crystals were form II. At even higher supersaturations $S_I = 3.1-4.5$ the crystals were form II as well. However, the induction time in these experiments was less than 10 s, which might indicate that nucleation and growth already take place during the mixing of solution and antisolvent under inhomogeneous supersaturation conditions. Therefore, these experiments were not considered in Figure 6.

The shape of form II crystals is a function of the supersaturation ratio. Up to an initial supersaturation of $S_I = 2.3$ form II crystals had a platelike shape, while above that the crystals had a needle-like shape. The microscopic images in Figure 7 show crystals of form I with prism shape, and form II with platelike and needle-like shape, respectively. It appears that, at higher supersaturation ratios, the relative growth rate of the top faces of the needle crystals compared to that of the side faces increases.

Overall, it can be seen in Figure 6 that with an increase of the supersaturation ratio the obtained product changes from form I to form II, while the water volume fraction did not influence the obtained polymorphs.

Solvent-Mediated Transformation Rate. The transformation process from form II to form I was completed in 30 min at $S_I = 2.2$, $x_{v,w} = 0.6$ and $S_I = 3.3$, $x_{v,w} = 0.7$, and around 35 min

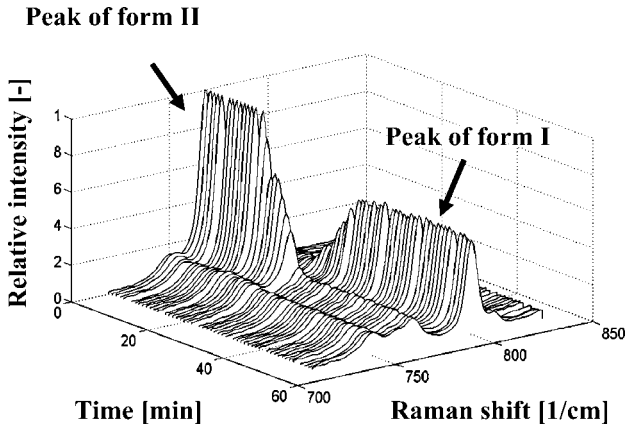

Figure 8. Inline measurement of the transformation from form II to form I by Raman spectroscopy as a function of time at an initial $S_I = 3.3$, $x_{v,w} = 0.7$ (298 K).

at $S_I = 4.5$, $x_{v,w} = 0.8$. Figure 8, which was obtained from inline measurement at $S_I = 3.3$, $x_{v,w} = 0.7$ by Raman spectroscopy, indicates the decrease in form II crystals and an increase in form I crystals. At the start the antisolvent crystallization resulted in a suspension containing only form II crystals. The peak intensity of form I started to increase around the eighth minute, that is, form I appeared. Around the 15th minute the peak intensity of form II started to decrease, indicating dissolution of form II. By assuming that the transformation is limited by the growth rate of form I rather than the dissolution rate of form II,[8] the concentration approaches the saturation concentration of form II. After another 5 min, 50% of form II transformed into form I. Finally, the transformation was completed in 32 min, where no form II could be detected.

The transformation of *o*-ABA is a relative fast process; several orders of magnitude shorter compared to amino acid L-histidine and L-glutamic acid. At 298 K the transformation processes of L-glutamic acid[10] and L-histidine[9] were completed in around 8 and 70 h, respectively. The rapid transformation of *o*-ABA could be caused by the larger solubility difference of the *o*-ABA polymorphs compared to L-glutamic acid and L-histidine.

Growth Rate Measurement. The growth rate of both forms was measured in an experiment of antisolvent crystallization/transformation starting at an initial $S_I = 1.6$, since concomitant polymorphism was observed at this supersaturation. In Figure 9, four frames from a sequence of microscopic images recorded every 10 s illustrate the appearance, growth, and transformation of forms I and II crystals. It should be noted that the time indicated on each image does not include the induction time. Figure 9a, taken just after the detection of the first crystals, shows the crystals of form I (prism shape) and II (platelike shape) appearing simultaneously. The apparent shape difference of the form I crystals in Figure 9 is due to different orientations of the crystal under the microscope. Figure 9b shows the crystals of both forms growing. Figure 9c,d shows the metastable form II dissolving, while the stable form I is still growing. This proves that concomitant polymorphism of *o*-ABA is due to the competitive nucleation and growth and not due to transformation of form II into form I.

This conclusion is not consistent with Ostwald's rule of stages, according to which the metastable polymorph forms first, followed by a transformation to the more stable polymorph.[11] Many cases[9,12] of directly crystallizing more stable forms or concomitant polymorphs indicate that Ostwald's rule of stages is not a general physical law. If the nucleation rates and growth

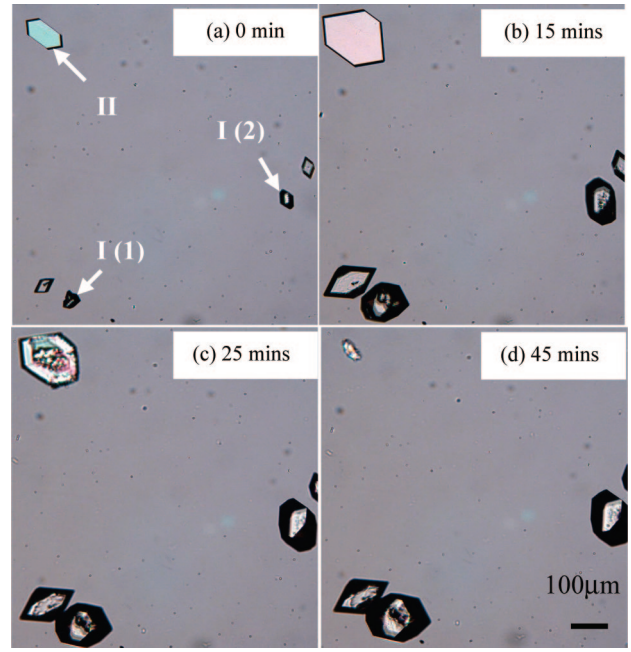

Figure 9. Four frames from a sequence of microscopic images showing the appearance, growth, and transformation of form I (prism shape) and form II (platelike shape) crystals at initial $S_I = 1.6$, $x_{v,w} = 0.5$. Time was counted after the induction time. The crystals indicated by arrows were selected for the estimation of growth rate.

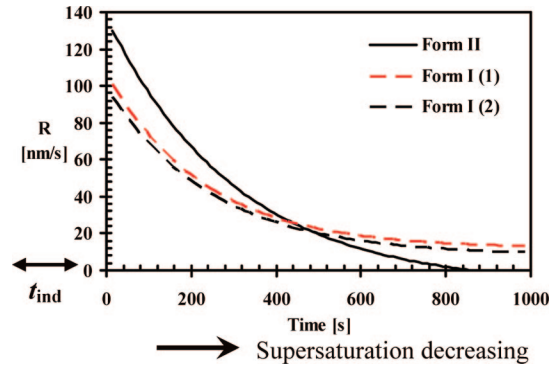

Figure 10. The estimated growth rate of form I and II crystals as a function of time at initial $S_I = 1.6$, $x_{v,w} = 0.5$. Time was counted after induction time. The supersaturation ratio decreases with the time.

rates (JR^3) of stable and metastable form are equal, their appearance of probabilities will be nearly the same. Under such conditions, concomitant polymorphism will take place.

From the sequential images, two crystals of form I and one crystal of form II indicated by arrows in Figure 9a were selected for growth rate estimation of both forms under equal conditions. The surface areas of both crystals were measured using the software of Image-Pro Plus. The lengths L of the crystals, defined as the diameter of the equivalent square, were calculated from the areas. Figure 10 shows the growth rate R defined as $R(t) = dL/2dt$ versus time. It is found that, compared to form I, the growth rate of form II initially was larger. The form II growth rate decreases more steeply until the eighth minute, after which $R_I > R_{II}$. After around 14 min the growth of the form II crystal stopped, while the form I crystal continued growing with a constant growth rate. Later, the form II crystal started to dissolve, while the form I crystal remained growing with a constant rate. The measured growth rate of the form I crystals agrees quite satisfactorily.

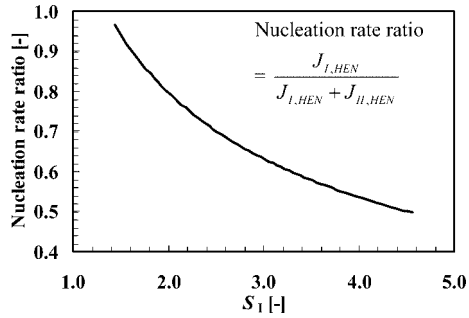

Figure 11. Calculated rate ratio of heterogeneous nucleation as a function of initial supersaturation ratio S_I.

Because the solute concentration is consumed by the growing crystals, the supersaturation ratio decreases as the time passes. It can be concluded that the growth rates at high supersaturation $R_I < R_{II}$ while at low supersaturation $R_I > R_{II}$. Even though the supersaturation of form II (S_{II}) is lower, at sufficiently high supersaturations the growth rate of form II will be higher than that of form I.

It is interesting to further estimate at which supersaturation ratio the growth rates of forms I and II are equal. As shown in Figure 10, at the dissolution point of form II the supersaturation ratio S_I was 1.2 calculated from the known solute concentration, that is, the solubility of form II, and the growth rates of form I crystals (1) and (2) were 14 and 11 nm/s, respectively. By assuming the growth mechanism was spiral growth, for which the growth order can be assumed $n = 2$, the overall growth constants k_G of form I were calculated using eq 6. Using this k_G the supersaturation ratio at which $R_I = R_{II}$ was consequently estimated to be $S_I = 1.3$. As a check, the supersaturation ratio S_I just after the detection of the first crystals, that is, $t = 0$ in Figure 10, was also estimated using the determined k_G, and S_I was around 1.57, which was reasonably lower than the initial supersaturation ratio of 1.6. It can be concluded that under these experimental conditions the metastable form II grows faster than the stable form I above $S_I = 1.3$.

Discussion

Besides the growth rates the competitive nucleation rates of both forms should be known to explain the dependence of polymorphic behavior of *o*-ABA on the supersaturation ratio. Usually, heterogeneous nucleation occurs more readily in solution crystallization, except that at extremely high supersaturations homogeneous nucleation could be the dominant nucleation.[13] Equations 2 and 3 were used to calculate the homogeneous nucleation rates of both polymorphs. The interfacial energies for HON as a function of water volume fraction were estimated according to the Mersmann equation with the molecular volume: $v_I = 1.62 \times 10^{-28}$ m^3 and $v_{II} = 1.66 \times 10^{-28}$ m^3. The calculated values of HON rate were extremely low, and it was therefore assumed that the nucleation proceeded according to a heterogeneous nucleation mechanism.

To calculate the HEN rate, the effective interfacial energy was estimated using eq 5 with $\psi = 0.2$. In Figure 11, the theoretical rate ratio for HEN, defined as $J_I/(J_I + J_{II})$, is plotted as a function of initial supersaturation ratio S_I. It was found that at low supersaturation J_I was much larger than J_{II} because the ratio approaches 1. The nucleation rate ratio decreased with increasing the supersaturation ratio and at high supersaturation J_I was almost equal to J_{II}. However, these data should be taken with care due to inaccuracies possible in the values of γ and ψ.

According to the theoretical results of nucleation rates and experimental results of growth rates presented in the previous section, the polymorphic behavior of *o*-ABA can be explained. At low supersaturation ratio, theoretically $J_I > J_{II}$ and experimentally $G_I > G_{II}$, the obtained crystals from antisolvent experiments were only form I. As the supersaturation ratio increases, the nucleation rates of both forms were closer and so were the growth rates, so concomitant polymorphism took place. At an even higher supersaturation ratio, theoretically $J_I \approx J_{II}$ and experimentally $G_{II} > G_I$, pure form II was obtained in the first instance followed by a relatively fast transformation into form I. It might also indicate that the competitive growth rates of polymorphs seem to be the governing parameter in the determination of the polymorphic fraction.

Moreover, the polymorph crystallization of *o*-ABA is probably affected by the speciation in solution as well, since the crystal structure of form I contains both the zwitterionic species and the nonzwitterionic species, while form II and III only contain the nonzwitterionic species. The effect of speciation on the polymorphs of *o*-ABA will be investigated in the future.

Conclusions

The antisolvent crystallization of *o*-ABA was performed in batch experiments at 298 K by mixing an ethanol solution of *o*-ABA with water as antisolvent. The solubility of form I decreases as a function of water volume fraction at 298 K. The metastable form II has a higher solubility than form I, with a ratio of $c^*_{II}/c^*_I = 1.20$.

In experiments of antisolvent crystallization, the supersaturation ratio and interfacial energy were varied by changing the initial concentration of *o*-ABA in ethanol and the water volume fraction. Raman spectra of forms I and II showed distinct differences that could be used to identify the obtained polymorphs. Antisolvent crystallization results in form I crystals at low supersaturations, form II at high supersaturations, and concomitant polymorphs at intermediate supersaturations. A similar effect of interfacial energy was not observed. Mixing of the reactants was assumed to have no effect on the experimental results, because the mixing time was much shorter than the shortest induction time.

The growth rate of both forms was measured in an experiment of antisolvent crystallization starting at an initial $S_I = 1.6$ and antisolvent fraction $x_{v,w} = 0.5$, which proves that concomitant polymorphism of *o*-ABA is due to the competitive nucleation and growth rates of forms I and II and not due to transformation of form II into form I. This conclusion indicates that the Ostwald's rule of stages was not observed in the antisolvent crystallization of *o*-ABA.

From the sequential images, the growth rates of form I and II crystals were estimated under equal conditions, and the nucleation rates were calculated according to the classical nucleation theory. At low supersaturation ratio, theoretically $J_I > J_{II}$ and experimentally $G_I > G_{II}$, and only stable form I was obtained. With the increase of supersaturation ratio, the nucleation rates of both forms approached and so were the growth rates, which resulted in concomitant polymorphism. At an even higher supersaturation ratio, theoretically $J_I \approx J_{II}$ and experimentally $G_{II} > G_I$, and the suspension right after the induction time contained only metastable form II crystals.

Next to that, a relatively fast solvent-mediated transformation occurs, even at high water volume fractions. In the case of *o*-ABA, although antisolvent crystallization under conditions of high supersaturations results in the formation of concomitant

polymorphs or the undesired metastable form II the stable form I can be readily obtained at 298 K due to this rapid transformation.

Acknowledgment. The authors thank NWO and SENTER for their financial support to this project.

References

(1) Bernstein, J.; Davey, R. J.; Henck, J. O. *Angew. Chem., Int. Ed.* **1999**, *38*, 3440–3461.
(2) Palafox, M. A.; Gil, M.; Nunez, J. L. *Vib. Spectrosc.* **1993**, *6*, 95–105.
(3) Harris, R. K.; Jackson, P. *J. Phys. Chem. Solids* **1987**, *48*, 813–818.
(4) Ojala, W. H.; Etter, M. C. *J. Am. Chem. Soc.* **1992**, *114*, 10288–10293.
(5) Kashchiev, D.; van Rosmalen, G. M. *Cryst. Res. Technol.* **2003**, *38*, 555–574.
(6) Mersmann, A. *J. Cryst. Growth* **1990**, *102*, 841–847.
(7) Mullin, J. W. *Crystallization*; Butterworths: Oxford, U.K., 2001.
(8) Davey, R. J.; Cardew, P. T.; Mcewan, D.; Sadler, D. E. *J. Cryst. Growth* **1986**, *79*, 648–653.
(9) Roelands, C. P. M.; Jiang, S.; Kitamura, M.; ter Horst, J. H.; Kramer, H. J. M.; Jansens, P. J. *Cryst. Growth Des.* **2006**, *6*, 955–963.
(10) Ono, T.; ter Horst, J. H.; Jansens, P. J. *Cryst. Growth Des.* **2004**, *4*, 465–469.
(11) Ostwald, W. *Z. Phys. Chem.* **1897**, *22*, 289–330.
(12) Kitamura, M. *Cryst. Growth Des.* **2004**, *4*, 1153–1159.
(13) Roelands, C. P. M.; ter Horst, J. H.; Kramer, H. J. M.; Jansens, P. J. *Cryst. Growth Des.* **2006**, *6*, 1380–1392.

CG070517N